CFD MODELLING OF MACRO-SEGREGATION AND SHRINKAGE IN LARGE DIAMETER STEEL ROLL CASTINGS: A COMPARISON ON SEN AND DLP TECHNIQUES

Laurentiu Nastac[1*] and Kevin Marsden[2]

[1] THE UNIVERSITY OF ALABAMA, Department of Metallurgical and Materials Engineering, P. O. Box 870202, Tuscaloosa, AL, 35487-0202, USA
[2] Whemco, Inc., 5 Hot Metal Street, Pittsburgh, PA, 15203-2351, USA

*Corresponding author, E-mail address: lnastac@eng.ua.edu

ABSTRACT

The reduction of macro-segregation and shrinkage during up-hill teeming of medium carbon ingots has always presented a technical challenge. Whemco has improved the processing techniques for steel roll ingots by balancing the casting heat input and the heat extraction rate from the roll surface. By injecting a dilute alloy through a submerged entry nozzle (SEN) into the roll, or through direct ladle pouring (DLP), further alleviated undesirable consequences of macro-segregation. Thus, centreline and mid-radius segregation can be significantly minimized.

The objective of this study is to determine the effects of DLP technique and compare them with the SEN technique on the centreline and mid-radius segregation, as well as solidification behaviour in the transition region between the outer shell and diluted core. To accomplish this objective, a multi-phase multi-component CFD model was applied for predicting the macro-segregation and shrinkage under various casting conditions for a 65-tonne 1.625 m diameter steel roll.

NOMENCLATURE

SEN   submerged entry nozzle
DLP   direct ladle pouring

INTRODUCTION

In this study, a numerical framework for predicting macro-segregation in roll ingot processes based on a computational fluid dynamics (CFD) code was further refined and applied. The multiphase CFD code solves for the temperature, flow and solute balance using a multi-component alloy system approach. Several macro-segregation models have been proposed in the literature and the most relevant ones are presented in [1-10]. These models were developed and validated only for binary alloy systems and they do not take into account all of the transport phenomena at both micro- and macro-level that can take place during ingot casting and solidification.

The ingot segregation model was tailored for roll ingots. The multi-phase modelling development effort includes up-hill teeming of the base alloy, SEN and DLP top pouring of the dilute alloy, species transfer during filling, and multi-component segregation during solidification. The model customization also includes the development and implementation of boundary conditions of each process, meshing, and thermo-physical solidification and segregation properties of the base and diluted steel alloys.

MODEL DESCRIPTION

A multi-scale model capable to simulate macro-segregation macro- and micro-shrinkage during ingot casting and solidification of multi-component alloys was developed and implemented into a CFD code. The model features includes viscous k-ε with standard wall functions, species transport and modified Scheil-based solidification sub-models. The Scheil micro-segregation equation with back-diffusion correction was used to account for diffusion in the solid phase in a multi-component system [11-14]. Thus, the model can properly take into account the microstructure characteristics of the steel alloys and the cooling conditions in the cast rolls. The CFD model for predicting macro-segregation during solidification of various roll and ingot casting processes was developed by solving in a fully coupled mode for the volume fraction of phases (air and steel mixture), temperature, flow and solute balance in steel alloy systems [15, 16].

The flux boundary conditions at the roll surface were determined based on the experimental temperature measurements for a 65-tonne 1.625 m diameter steel roll [15]. All the thermo-physical properties and solidification parameters of the steel alloys used in the current simulations are functions of temperature.

The model was previously validated (see details in Refs. [15, 16]) using the numerical results published by Prescott and Incropera [17], Beckermann and Viskanta [18] and Rappaz and Voller [19] and the comparison against the experimental measurements shown in [15, 16, 20]. Additional validation of the model is shown in this study.

RESULTS

The process and material parameters for the studied SEN and DLP rolls are as follows:
Up-hill teeming, top insulation, cast iron chills, improved (double) insulation for the mould side;
Constant top inlet velocity: $V_{in} = 6.478$ m/s (air and dilute alloy allowed to outflow);
SEN (75 mm nozzle diameter) or DLP;
SEN dilute alloy composition: 0.21 wt.% C, 0.55 wt.% Cr, 0.27 wt.% Mo;

DLP dilute alloy composition: 0.35 wt.% C, 2.55 wt.% Cr, 0.15 wt.% Mo;
Up-hill teemed composition of SEN roll: C = 0.44 wt.%, Cr = 4.06 wt.%, Mo=0.64 wt.%;
Up-hill teemed composition of DLP roll: C = 0.47 wt.%, Cr = 4.13 wt.%, Mo=0.70 wt.%.

A thorough investigation was performed for the SEN and DLP cases. The simulation results are presented in the following subsections (Figures 1-12).

SEN Case

Figure 1 shows the Cr profile at the end of the back-feeding (*e.g.*, dilution) process (time = 10800s). Figures 2 to 4 present the simulation results for the SEN using a cast iron chill case at the end of solidification (time = 97000s). The segregation profiles for C, Cr and Mo in Fig. 3 show minimum centreline and mid-radius segregation (*e.g.,* A-type channel segregation). There is some predicted centreline segregation for C, Cr and Mo closed the top of the roll and especially in the riser. This can further be reduced by controlling the heat extraction rate in the roll.

Niyama criterion (Figure 4a) is applied to estimate the tendency to develop shrinkage porosities in the roll casting. The predictions show the formation of severe shrinkage porosities in the base alloy shell close to the riser junction and at the roll bottom. This is because of relatively low temperature gradients and high cooling rates in these regions. These predictions were confirmed by experimental measurements and NDE inspection.

The temperature gradients (G, in K/m) (Figure 4b) are calculated at the liquidus temperature (TL). The columnar-to-equiaxed transition (CET) was estimated by using a critical temperature gradient (G_{cr}) below which equiaxed grains can start to nucleate and grow. Typically, G_{cr} is alloy chemistry dependent and process independent and its value can be estimated via unidirectional solidification experiments. Grain refinement will also affect the CET formation. The assumed G_{cr} value for the current cast roll is 3000 K/m. The predicted CET compared favourably with the experimental CET in this roll (see Fig. 4b for the predicted equiaxed zone and Ref. [15] for the experimental CET).
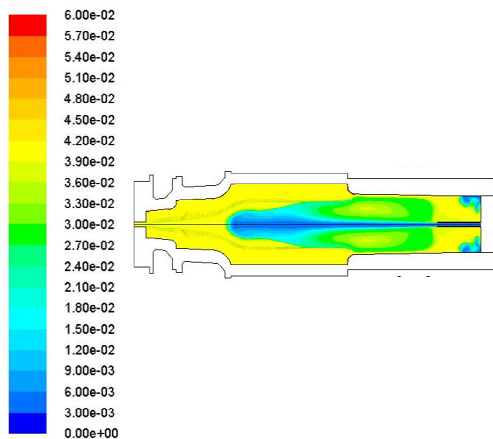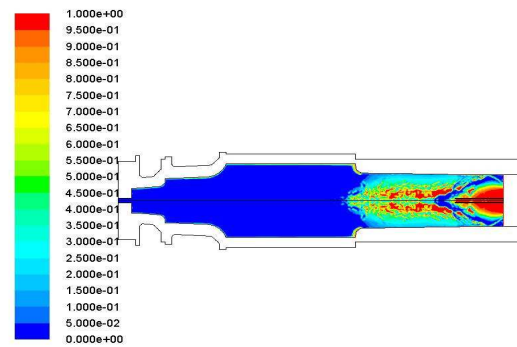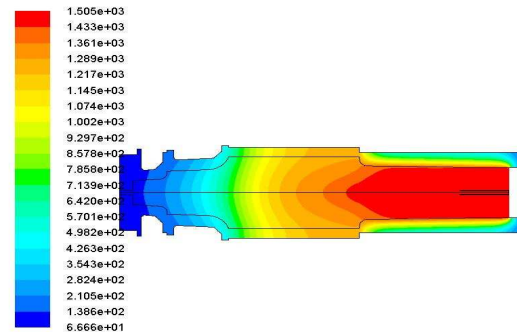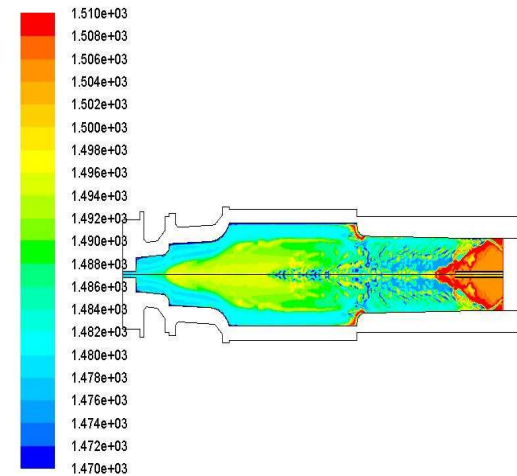

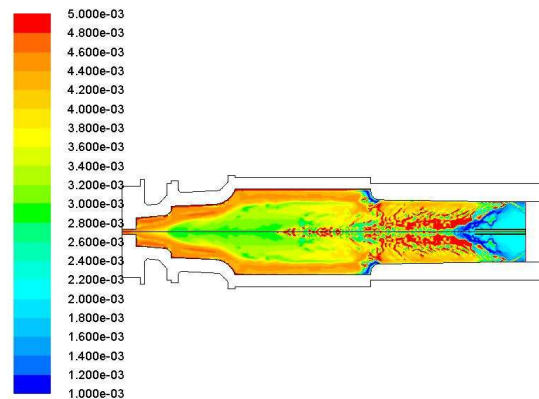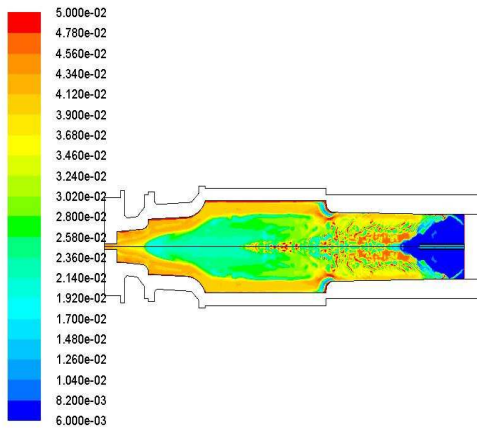**Figure 1**: SEN case: Cr profile at the end of dilution process.
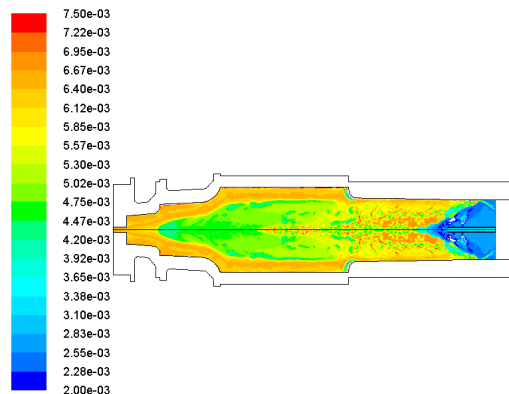

(a)

(b)

(c)

Figure 2: SEN case: Liquid fraction (a) temperature (in deg. C) (b) and liquidus temperature (in deg. C) (c) distributions at the end of solidification (time t = 97000s).
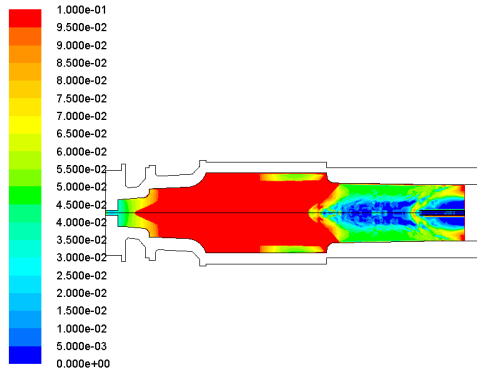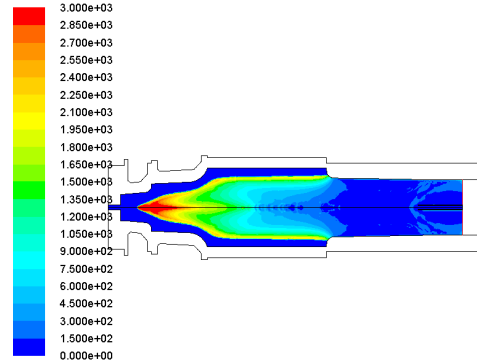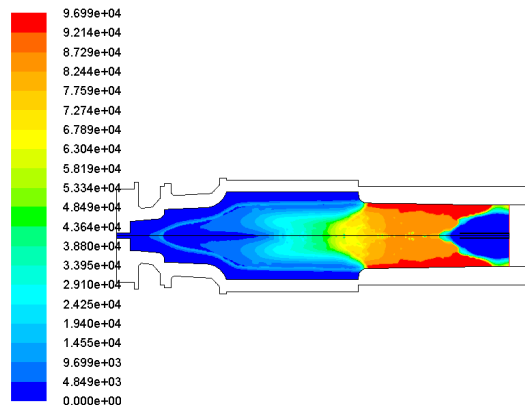

(a)

(b)

(c)

Figure 3: SEN case: Distributions of (a) C, (b) Cr, and (c) Mo mass fractions at the end of solidification (97000s).
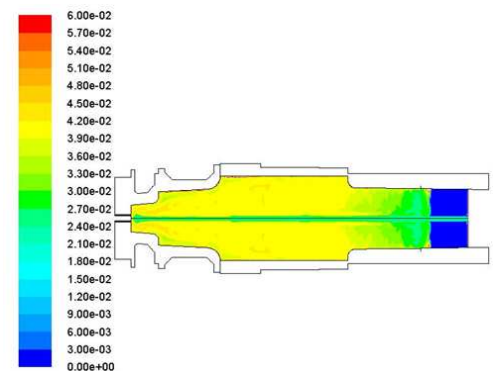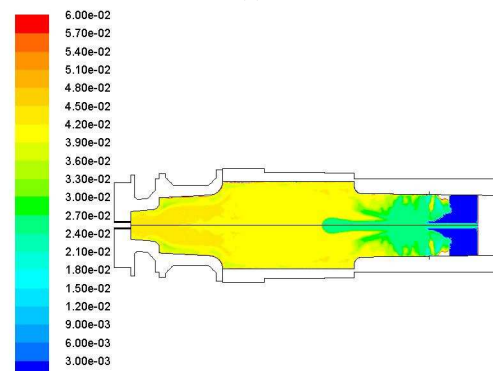

(a)

(b)

(c)

Figure 4: SEN case: Distributions of (a) Niyama values, (b) Temperature gradients at liquidus temperature (T_L), in K/m) and solidification time (s) (time t = 97000s).
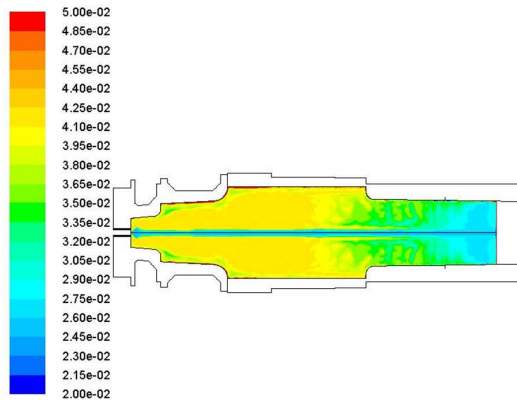
DLP Case

Figure 5 shows the Cr profile at the end of the dilution process (time = 4800s (~1.5 hours)). A comparison between laminar and turbulent flow conditions is also provided in Fig. 5. The surface turbulence that develops during the DLP dilution process (Fig. 5b) may absorb a significant amount of the jet momentum/ energy and thus the penetration depth may be substantially decreased when compared with the SEN dilution process (Fig. 1). Figures 6 to 8 present the simulation results for the DLP case toward the end of solidification (time = 109000s (~30 hours)). Slightly lower temperature gradients and longer local solidification times are predicted for the DLP case. This is because of the shapes of the side chills and their insulation thicknesses are somewhat different in the DLP case when compared with the SEN case.
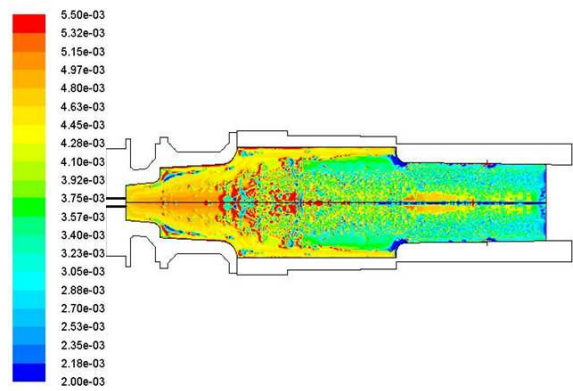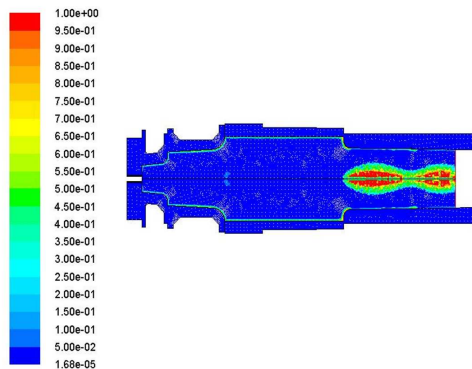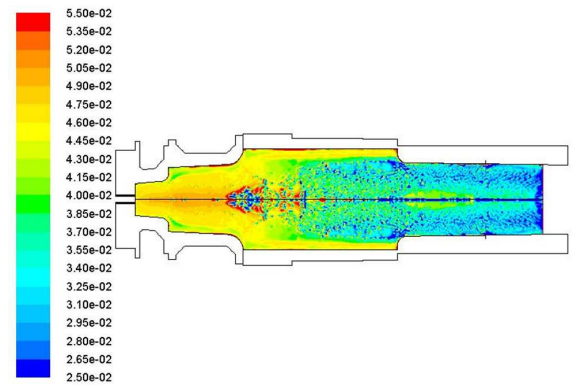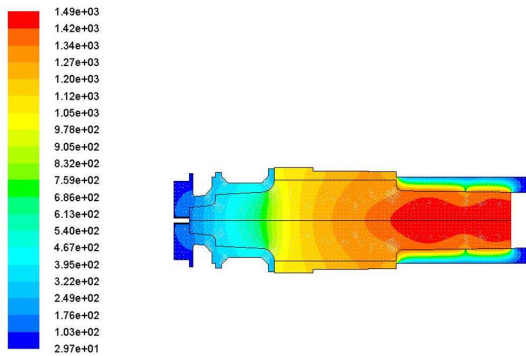

(a)

(b)

3

(c)

Figure 5: DLP case: Cr profile under laminar (a) and highly turbulent (b) flow conditions during the back-feeding process and (c) Cr profile at the end of dilution process (under laminar flow conditions).
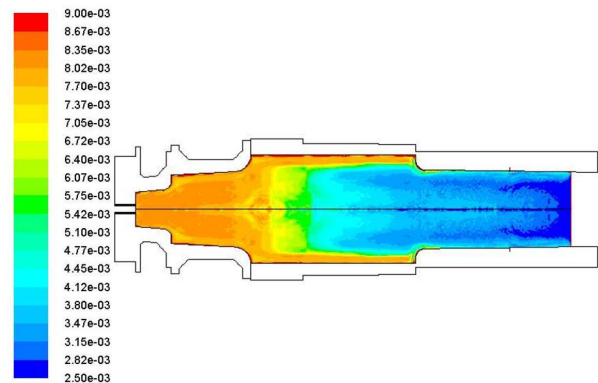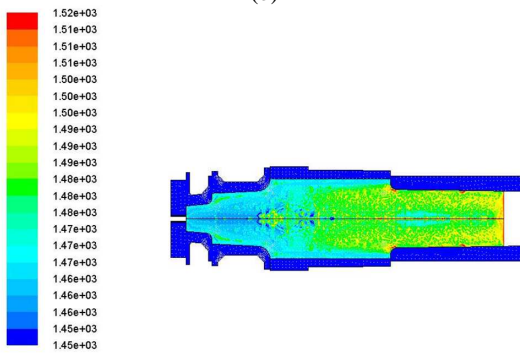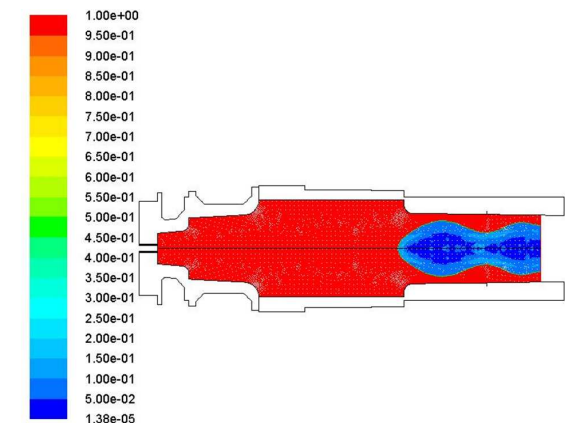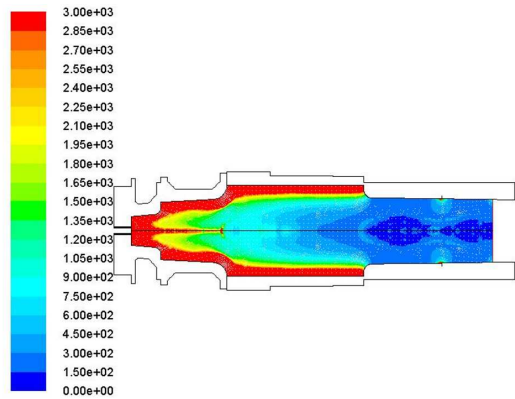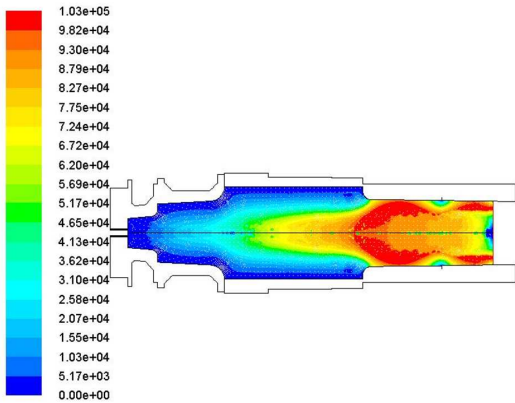

(a)

(b)

(c)

Figure 6: DLP case: Liquid fraction (a), temperature (in deg. C) (b) and liquidus temperature (in deg. C) (c) distributions at the end of solidification (time t = 97000s).
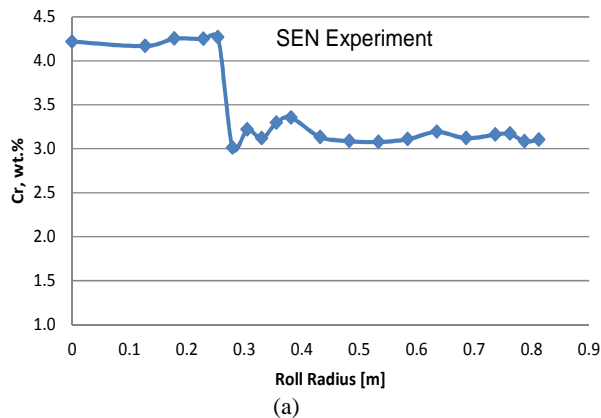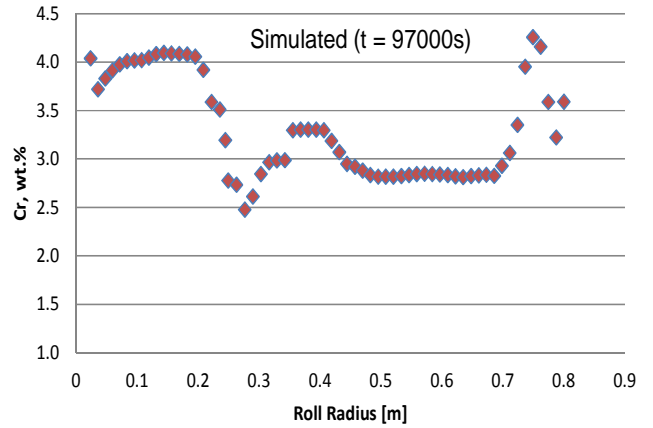

(a)

(b)

(c)

Figure 7: DLP case: Distributions of (a) C, (b) Cr, and (c) Mo mass fractions at the end of solidification (time t = 109000s).

(a)

(b)

(c)

Figure 8: DLP case: Distributions of (b) Niyama values, (b) Temperature gradients at liquidus temperature (T_L), in K/m) and solidification time (s) (at time t = 109000s).

Cr and Mo Segregation Profiles: Comparison of SEN and DLP Cases

Figures 9 and 10 show a comparison of the segregation profiles of predicted and experimental Cr and Mo for the SEN case. Figures 11 and 12 show a comparison of the segregation profiles of predicted and experimental Cr and Mo for the DLP case. The simulation results compare favourably with the experimental measurements. The overall dilution and mixing process is predicted well for both dilution processes. The fusion zone (the distinct area between the shell and core zones) is distinctive in the SEN process (Figs. 9 and 10) while indeterminate in the DLP process (Figs. 11 and 12). Also, the Cr segregation is higher in the DLP than in the SEN.
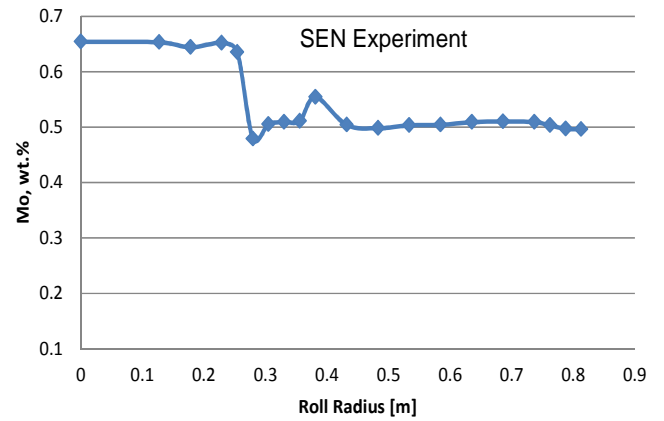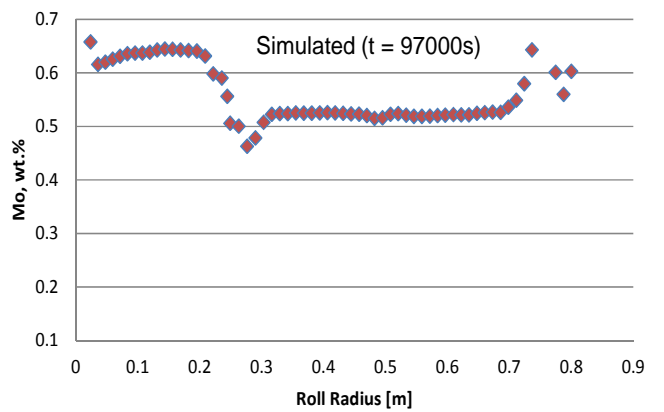

(a)

(b)

Figure 9: SEN case: Comparison of experimental Cr (in wt. %) (a) and predicted Cr mass fractions (b) near the top of the roll body.

(a)

(b)

Figure 10: SEN case: Comparison of experimental Mo (in wt. %) (a) and predicted Mo mass fractions (b) near the top of the roll body.
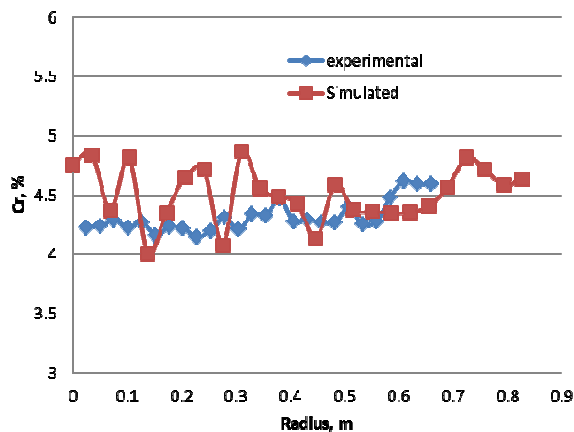
Figure 11: DLP case: Comparison of experimental Cr (in wt. %) (a) and predicted Cr mass fractions (b) near the top of the roll body.
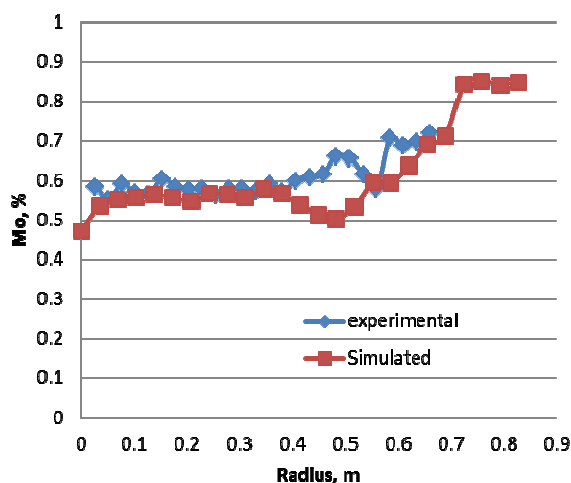

Figure 12: DLP case: Comparison of experimental Mo (in wt. %) (a) and predicted Mo mass fractions (b) near the top of the roll body.

CONCLUDING REMARKS AND FUTURE WORK

A numerical modelling approach for predicting macro-segregation in casting was developed and implemented into a CFD code and further refined in the current work. The model validation was performed using experimental measurements for a 65-tonne 1.625 m diameter steel roll that was cast using both SEN and DLP techniques. .

The simulation results compare reasonably well with the experimental measurements. It was determined that the overall dilution/mixing behaviour is comparable for the DLP predictions and experiments. It was also determined that surface turbulence that develops during the DLP dilution process absorbs some of the jet momentum/ energy and thus the penetration depth is decreased when compared with the SEN dilution process; also bubbles and oxides (bi-films) that form during top pouring may be entrained/ entrapped in the mushy zone. Thus, the SEN approach is recommended as a feasible top dilution process. The dilute alloy is hotter than the core alloy; mixing takes place in the radial direction. Stratification may also occur, which will decrease mixing during solidification. Because of the decrease in the penetration

depth and mixing, the segregation of C, Cr, and Mo is expected to be higher in the DLP case. To improve both the penetration depth and the mixing, it is recommended the use of a dilute alloy with similar or lower TL and superheat than that of the core alloy.

Future work will include conceptual mould designs to minimize macro-segregation and shrinkage at the centreline and at the shell/core interface of the cast rolls.

REFERENCES

[1] STEFANESCU, D. M.(2002): Science and Engineering of Casting Solidification, *Kluwer Academic/Plenum Publishers*.

[2] BENNON, W. D.; INCROPERA, F. P. (1987): *Int. J. Heat Mass Transfer*, **30**, 2161-2171.

[3] FELLICELLI, S. D.; HEINRICH, J. C.; POIRIER, D. R. (1991): *Met. Trans*, **22B**, 847.

[4] DIAO, Q. Z.; TSAI, H. L. (1993): *Met. Trans*, **24 A**, 963.

[5] SCHNEIDER, M. C.; BECKERMANN, C. (1995): *Met. Trans*, **26A**, 2373.

[6] CHANG, S.; STEFANESCU, D. M. (1996): *Met. Trans*, **27A**, 2708.

[7] OLDENBURG, C.; M.; SPERA, F. J. (1992): *Numer. Heat Transfer B*, **21**, 217.

[8] FLEMING, M. C.; NEREO, G. E. (1967): *Trans. AIME*, **239**, 1449.

[9] GULLIVER, G. H. (1913): *J. Inst. Met.*, **9**, 120.

[10] SCHEIL, E. (1942): *Zeitschrift Metalkde.*, **34**, 70.

[11] NASTAC, L. (2004): Modeling and Simulation of Microstructure Evolution in Solidifying Alloys, *Springer, New York*.

[12] NASTAC, L.; STEFANESCU, D. M. (1993): "A Model for Solute Redistribution during Solidification of Plate, Columnar or Equiaxed Grains," *Met Trans*, **24A**, 2107-2118.

[13] CLYNE, T.; KURZ, W. (1981): *Met. Trans*, **12A**, 965.

[14] GANGULY, S.; CHAKRABORTY, S. (2006): *Met. Trans*, **37B**, 143-145.

[15] NASTAC, L. (2010): "CFD Modelling of Macro-Segregation during Solidification of Superalloy Castings," *Proceedings of the 2nd International Symposium on Cutting Edge of Computer Simulation of Solidification and Casting (CSSC2010)*, Sapporo, Japan, February 2-6, published in *ISIJ*, Japan, December 15.

[16] NASTAC L. (2011): "Computational Fluid Dynamics Modelling of Macro-Segregation and Shrinkage in Large Diameter Steel Roll Castings," *Met Trans*, **42B**, 1231-1243.

[17] PRESCOTT, P.J.; INCROPERA, F.P. (19940: *J. of Heat Transfer*, **116**, 735-749.

[18] BECKERMANN, C.; VISKANTA, R. (1988): *Physicochemical Hydrodynamics*, **10**, 195-213.

[19] RAPPAZ, M.; VOLLER, V. (1990): *Met. Trans*, **21A**, 749.

[20] NASTAC L.; MARSDEN M. (2012): "CFD Modelling and Simulation of Macro-Segregation and Shrinkage in Large Diameter Steel Roll Castings: Chill Study," *Proceedings of the 1st International Conference on Ingot Casting Rolling and Forging, (ICRF2012)*, Aachen, Germany, Eurogress, June 3-7.